
*17th World Conference on Earthquake Engineering, 17WCEE*
*Sendai, Japan - September 13th to 18th 2020*

# ROCKING vs. CONVENTIONAL SEISMIC ISOLATION: COMPARATIVE ASSESSMENT OF ASYMMETRIC BRIDGES IN A DESIGN CONTEXT

I.M. Thomaidis [(1)], A.J. Kappos [(2)], A. Camara [(3)]

[(1)] *PhD Candidate, City, University of London, United Kingdom, ioannis.thomaidis@city.ac.uk*
[(2)] *Professor, Khalifa University, United Arab Emirates, andreas.kappos@ku.ac.ae*
[(3)] *Senior Lecturer, City, University of London, United Kingdom, alfredo.camara@city.ac.uk*

## *Abstract*

Rocking seismic isolation has emerged as a promising and potentially improved alternative to the generally well-performing conventionally isolated bridges. Previous works on the topic compared the seismic response of bridges designed with the conventional isolation techniques with that of bridges in which piers are allowed to rock freely on the foundation and on the deck, respectively ("structural" rocking), and have revealed the superior performance of rocking bridges both in terms of residual deformations and collapse prevention. However, in all these cases the height of the piers is the same, hence ignoring the important problem of the bridge irregularity in the rocking response. Moreover, only extreme earthquake events have been examined and the merits or drawbacks of rocking isolation under more likely to occur ground motions have not been explored. The present paper investigates the performance of an existing bridge with irregular configuration that is common in existing motorways in Europe; it is analysed employing two different design approaches: (a) conventional seismic isolation with Lead Rubber Bearings and (b) "structural" rocking isolation of the piers. The conventionally isolated bridge is a modified version of an existing bridge, redesigned according to the current Eurocode 8 provisions, while in the "structural" rocking scheme realistic interface conditions are defined by means of a realistic value of the friction coefficient that allows the piers to rock without any supplementary damping or recentring devices (free-standing configuration). Rigorous 3D numerical models of the bridge that account for the abutment-backfill contribution are developed to analyse the response history of the proposed structures under pairs of 11 ground motions that match the design spectrum. Although both structures perform well under the seismic action, the deck of the rocking system develops generally larger horizontal displacements than the bridge with conventional LRB isolation. On the other hand, permanent displacements in the conventionally isolated system, albeit within code-prescribed limits, are larger than those in the rocking system, even when a conservative value for the coefficient of friction is selected. On the other hand, the bending moments in the deck supported by rocking piers increase, especially in the intermediate span where the differential uplift of the piers becomes significant. As expected, the rocking piers develop larger drifts than those in the conventionally isolated structure, mainly due to rigid body motion, while bending is reduced. However, increased bending moments are observed in the regions close to the rocking interfaces, therefore special attention should be paid to the reinforcement detailing of these zones.

*Keywords: bridge engineering, seismic isolation, conventional isolation, rocking isolation, finite element modelling*

 




## 1. Introduction

For over a century, the majority of earthquake-resistant bridge systems fell within two main categories, ductile pier and isolated bridges, both of which, although showed satisfactory behaviour in terms of collapse prevention, also suffer from a number of deficiencies related to their role in transport networks, such as loss of functionality after a strong seismic event and high cost of repair or maintenance. An alternative to the previous types of seismically resistant bridges is based on the concept of rocking mechanism, where all connections between the piers and the foundations as well as the deck, are removed and the piers are allowed to rock. Such behaviour in bridges has been thoroughly examined analytically [1, 2] by adopting some assumptions which are essential for formulating the rocking response, i.e. (i) the rocking problem is examined in two dimensions, (ii) sliding is avoided at any instant and (iii) all members are considered rigid. However, the two-dimensional analysis restrains the response to an impact-like motion, neglecting the phenomena of wobbling, rolling [3] or twisting of the bridge piers, which might occur during biaxial excitations, while the crude assumptions of no sliding at the rocking interfaces [4] and rigidity of all members [i.a. 5, 6] may lead to failing to properly capture the actual effect of rocking in all structural members. These problems can be tackled using numerical or experimental tools. Previous works using these techniques can be classified into two basic categories:

(1) When a monolithic connection is assumed between the rocking pier and the superstructure, Single Degree of Freedom (SDOF) models with a large mass at the top of the pier are usually adopted in numerical [i.a. 7] and experimental studies [i.a. 8].

(2) When a rocking joint is assumed between the rocking pier and the deck, numerical [i.a. 9] or experimental tools [i.a. 10] are utilised for models with a compressive force on top of the piers to represent the beneficial effect of the superstructure weight [11], while more comprehensive models with two rocking piers capped with a massive beam have also been developed numerically [6] or experimentally [i.a. 12].

However, the majority of these studies ignore the dynamic interaction among the different members, and all of them neglect the influence of the abutments [13]. To this end, a detailed comparison for a 5-span bridge with equal pier heights was conducted recently employing two different isolation techniques, i.e. (A) a conventionally isolated system and (B) a system where the piers are allowed to rock freely on the foundation ("structural" rocking isolation) [14]. In these two alternatives, the different structural members are identical and the piers are disconnected from the deck through bearings, thus rendering the system (B) a hybrid rocking solution. The performance of the systems was studied by considering pairs of 10 strong records that significantly exceed the design spectrum by two to seven times. The results revealed that system (B) avoided collapse in more cases than system (A). Moreover, the maximum moment at the pier foundation for system (B) was much lower than in structure (A). Another positive aspect observed in system (B) was that the residual displacements were negligible and, therefore, the structure is resilient and indeed ready-to-use even after the strongest earthquakes. However, this can be attributed to the special contact elements used in that work to prevent sliding (i.e. coefficient of friction was set equal to 10). Furthermore, it was observed for bridge (B) that the uplift of the rocking piers causes an increase in the bending moments at the end spans of the superstructure compared to bridge (A). However, this was not observed in the intermediate spans since the bridge was fully symmetric (all bridge piers are 10 m), thus the rocking piers are forced to uplift the same way considering synchronous movement. This is not the case in asymmetric configurations. Asymmetry has always been an issue in rocking structures as shown analytically for rigid frames [15] and bridges [2], due to the fact that the shorter piers are forced to undergo larger rotations (or uplifts) than the taller ones.

The aim of the present study is to identify the pros and cons of structural rocking isolation compared with a conventional isolation technique when implemented in a bridge that is asymmetric in elevation due to unequal pier heights. Consideration of asymmetry is essential as it appears to be a more detrimental case than that of a symmetric structure. In this context, this work can be considered as an extension of previous studies focusing on symmetric structures [e.g. 14]. The two isolation alternatives are implemented on an actual



 



asymmetric overpass. The rocking bridge consists of piers which are allowed to rock freely at both interfaces (pure free-standing configuration), while Lead Rubber Bearings (LRBs) are used in the conventionally isolated system in line with current Eurocode 8 (EC8) provisions [16]. Rigorous 3D numerical models of the entire bridge system are developed in the ABAQUS Finite Element (FE) software [17] and are subjected to pairs of 11 base excitations that match a design spectrum. Comparison is conducted in terms of displacements of the structural members and bending moments (BMs) of the superstructure. The BMs developed at the piers are compared for the two alternatives in order to detect potential vulnerable regions in the rocking case. Moreover, the recentring capability of the rocking system is examined considering realistic values for the friction coefficient ($\mu$) at the rocking interfaces.

## 2. Description of the Bridge Model and Analysis Outline

### 2.1 Typical highway overpass

An Egnatia Motorway overpass bridge located in Northern Greece is used as a case study, forming the basis for the developed numerical models, with due modifications depending on the analysed design alternative (conventionally isolated and structural rocking isolation). The original bridge is a 3-span 99-m long structure with a central span of 45 m and end spans of 27 m as well as a longitudinal slope of approximately 7%. Cross-sections of increased weight are used for the deck towards the abutments and the piers and a lighter box girder is selected for the spans (Fig. 1A and 1B). The superstructure is monolithically connected to the two single-column concrete piers (P1 and P2) of cylindrical cross section with diameter $D_p$ = 2.0 m and unequal heights ($h_{P1}$ = 5.4 m and $h_{P2}$ = 7.4 m). Movement in both directions is initially allowed at the abutments, while longitudinal and transverse displacements are restrained whenever a 100 mm and a 150 mm gap between the deck and the abutment is closed, respectively. The soil conditions are stiff formations corresponding to class 'B' according to EC8 site classification [16], and both piers are supported on surface footings with dimensions 9.0 × 8.0 × 2.0 m. The deck and piers are constructed using concrete grade B35 while abutments and foundations using B25. The original bridge was designed according to the provisions of the Greek Seismic Code with Peak Ground Acceleration (PGA) 0.16 g, site conditions 'B', importance factor 1.0 and behaviour factor 2.4 [18].

### 2.2 Finite element modelling

The seismic performance of the two alternative seismic isolation schemes is examined using ABAQUS [17], which can handle impact problems. This is done by applying the ground excitations separately for the two horizontal directions (i.e. longitudinal and transverse).

#### 2.2.1 Conventionally isolated system

A slightly modified version of the existing bridge is studied as shown in Fig. 1(A). The variant follows the dimensions of the actual bridge, but the structure is modified to a conventionally isolated system by separating the superstructure from the piers and the abutments through LRBs. Additionally, the piers are modified to rectangular cross-section with dimension 1.5 m to avoid wobbling and rolling effects that can affect piers with circular section [3]. The longitudinal slope of the superstructure is also ignored to simplify the model. The modified configuration is redesigned according to current EC8 provisions [16]. However, increased PGA is considered which is equal to 0.24 g due to the fact that the actual bridge was overdesigned for the actual PGA; the behaviour factors for longitudinal ($X$) and transverse ($Y$) directions are also modified considering that a seismically isolated configuration is examined, thus resulting in $q_{x\text{-}x(long)}$ = 1.0 and $q_{y\text{-}y(tran)}$ = 1.0. Elastic material properties are used for the different concrete grades. Specifically, for concrete grade B25 the characteristic compressive strength is set equal to $f_{ck}$ = 16 MPa and the mean Young's Modulus equal to $E_{cm}$ = 29 GPa, while the corresponding values for B35 are $f_{ck}$ = 30 MPa and $E_{cm}$ = 33 GPa. The specific weight and Poisson's ratio are defined 2.5 tonne/m$^3$ and 0.2, respectively, for both concrete grades. The LRBs are verified for (i) shear strain due to horizontal and vertical displacement as well as rotation, (ii) buckling stability, (iii) restoring capability and (iv) vertical load. The results indicate a total of 8 circular LRBs (i.e. 2 at each support position at a distance of 5.2 m) with dimensions 750 × 750 × 410 mm and



 



elastomer thickness $t_R$ = 170 mm as proposed by the manufacturer. The results from the modal analysis for the conventionally isolated system show that the first two physical modes of the system are translational and parallel to the transverse ($Y$) and longitudinal ($X$) directions with natural periods equal to $T_1$ = 2.09 s and $T_2$ = 2.07 s, respectively, achieving a mass participation factor above 85% for each case.

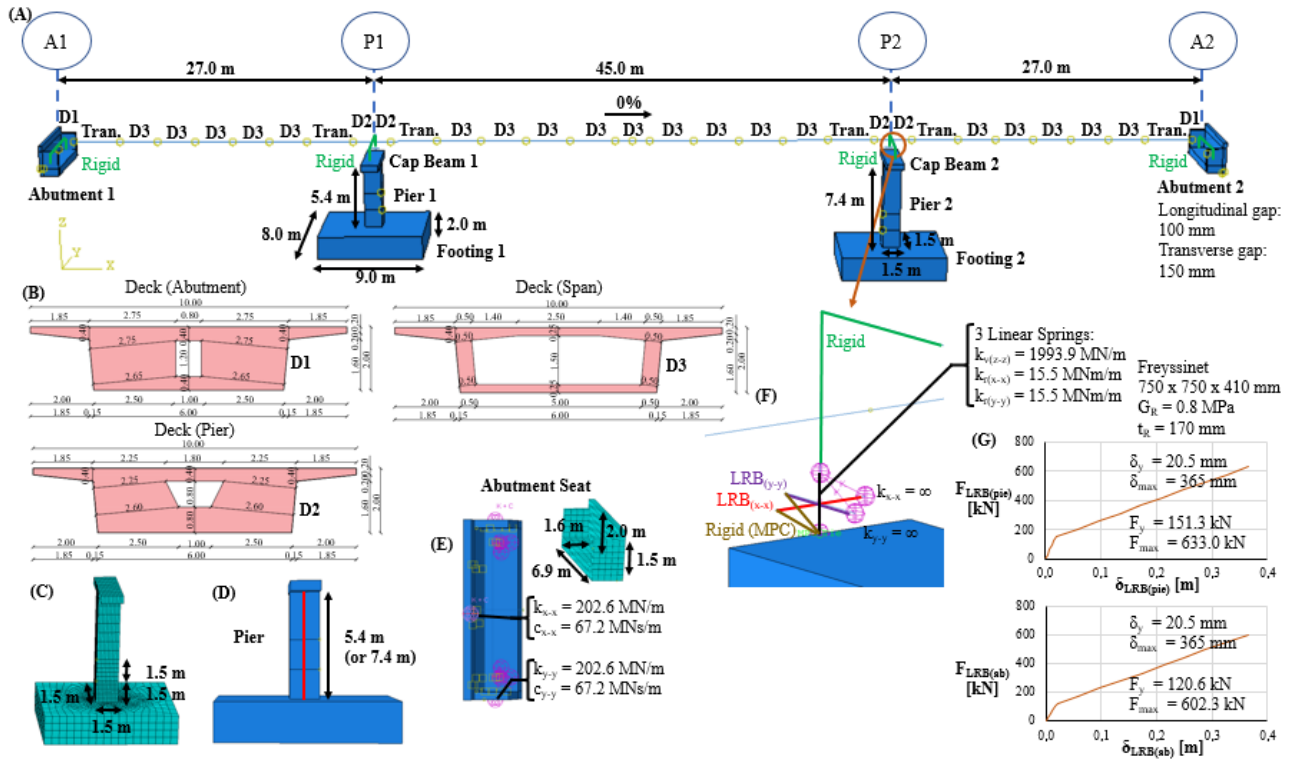


Fig. 1 – (A) Layout of the conventionally isolated bridge, (B) deck cross-sections, (C) mesh of foundation-pier-cap beam, (D) linear beam element of the piers, (E) layout of the abutment-backfill system, (F) model of the LRBs and (G) bilinear force-displacement behaviour of the LRBs located at the piers and abutments.

The FE model utilised for the dynamic analyses uses linear beam elements (B31) for the deck (located at the centroid of the box girder), while rigid elements are utilised to connect it with the LRBs as shown in Fig. 1(A). The deck is discretised in 34 parts to capture with more accuracy the BM distribution and the different cross-sections of the deck shown in Fig. 1(B). The system foundation-pier-cap beam is shown in Fig. 1(C). The piers are monolithically connected to the footings which consist of linear brick first-order elements with reduced integration (CED8R) of size 0.50 m. The piers are meshed with increasing size of the elements from bottom to top to capture in more accuracy increased stresses at the zones where damage is expected to occur. However, the transition between regions of different element sizes should be smooth and not differ by more than a factor of 2 to 4 in their volume [19]. Specifically, for a height of 1.5 m (i.e. the dimension of the square cross-section of the pier) cubic C3D8R elements of size 0.15 m are utilised, while a transition zone of 1.5 m height with equivalent elements of size 0.3 m is used to pass to the coarsest mesh for the rest of the pier utilising the same type of element with size 0.6 m. A cap beam with dimensions 1.5 × 5.2 × 1.0 m is introduced on top of each pier to support the LRBs [20] and follows the coarsest mesh of the pier (i.e. C3D8R with size 0.6 m). A B31 beam element with length equal to the height of the corresponding pier is integrated at the centroid of each pier, as shown in Fig. 1(D), in order to capture the flexural response of the element. The beam element is meshed according to the surrounding solid (i.e. zones with elements of 0.15 m, 0.3 m and 0.6 m), and it follows the movement of the latter by utilising the fully embedded option offered in ABAQUS [17]. It is noted that the beam element of the pier has negligible mass and stiffness compared to the rest of the structural members to avoid affecting the response of the structure. The abutment follows the dimensions of the actual bridge. However, only the seat of the abutment is modelled in detail



 



with C3D8R elements of size 0.3 m as shown in Fig. 1(E). The contribution of the abutment-backfill system is modelled through a linear spring ($k$ = 202.6 MN/m) [21] and a linear dashpot element ($c$ = 67.2 MNs/m) [22] at the longitudinal ($X$) and transverse ($Y$) directions. Interaction between the deck and the abutments is activated when the 100 mm and 150 mm longitudinal ($X$) and transverse ($Y$) gaps are closed, respectively, and is defined as a node-to-surface contact with a finite sliding option. In the normal direction, penetration of the deck in the abutments is not allowed at any case using the "Hard Contact" definition implemented in ABAQUS [17], while for the tangential behaviour the Coulomb friction expressed by a coefficient of friction $\mu$ = 0.9 [4] was used. The behaviour of each LRB is introduced in the model with 3 linear springs (1 axial and 2 flexural) and 2 horizontal truss elements (T3D2) to describe the shear behaviour of the isolator as shown in Fig. 1(F). Selection of truss elements (instead of e.g. linear springs) was made to integrate in the model the bilinear behaviour of the LRBs in order to detect potential permanent displacements of the superstructure. The 3 linear springs with length 0.41 m connect the cap beam with the deck and are introduced in the model with the axial ($k_v$) and flexural ($k_r$) stiffnesses [16, 23, 24, 25]. Due to the circular configuration of the LRB, the flexural resistance about the longitudinal ($X$) and transverse ($Y$) directions is the same as shown in Fig. 1(F). The 2 truss elements of each LRB have length 0.75 m. Rigid elements ("MPC Ties" available in ABAQUS [17]) are utilised to connect the cap beam with each truss element in order to transfer the pier movement to the LRBs, while connection of each LRB with the deck is accomplished through infinite stiffness springs which work only in the corresponding direction, as shown in Fig. 1(F). To account for the low confinement of lead in LRBs located at the abutments (due to the lower axial loads applied from the deck in this location compared to LRBs on top of the piers) the shear resistance $F_0 = F_{Ly}$ of abutment LRBs was reduced by assuming a 25% decrease in the yield stress of lead $f_{Ly}$ [24], thus resulting in two different load-displacement curves for the LRBs behaviour as shown in Fig. 1(G). The curves are constructed according to the manufacturer guidelines which follow the EC8 provisions [16]. The bottom surfaces of the abutments and the footings are restrained vertically ($Z$). Synchronous ground motions are applied to the whole volume of the footings separately for the longitudinal ($X$) and transverse ($Y$) directions.

### 2.2.2 Structural rocking isolation system

The variant with structural rocking isolation (Fig. 2A) is based on the conventionally isolated system with the necessary modifications due to the different isolation technique. Considering that no additional devices are utilised between piers and superstructure, the cap beam is removed and, therefore, the deck needs to be modelled with solid elements (C3D8R) in order to simulate the interface between the superstructure and the top surface of the rocking pier. Additionally, the dimensions of the shallow footings are modified to 3.0 × 3.0 × 1.2 m as shown in Fig. 2(A), since decreased moments occur at this member and smaller sections can be used compared to a conventionally isolated system [14]. Contact interactions are integrated in the model to ensure rocking motion of the piers with respect to the footings and the superstructure [i.a. 6, 9]. Thus, the piers exhibit a purely rocking response in which their weight and mass moment of inertia as well as the weight of the superstructure are the only restoring mechanisms of the system. The same concrete properties used in the conventionally isolated bridge are considered here.

Three different solid cross-sections are modelled for the superstructure as those shown in Fig. 2(B). The transition zone which was modelled for the conventionally isolated system (Fig. 1A) is neglected for simplification and the span section is used instead (Fig. 2A), while it is not expected to affect the results considerably. The deck is modelled with C3D8R elements of size 0.45 m, apart from the zones where the superstructure interacts with the abutments and the piers and a 0.15 m element is selected as shown in Fig. 2(C). The mesh for the system foundation-rocking piers is presented in Fig. 2(D). Cubic C3D8R elements of size 0.15 m are used for the footings, while the piers are meshed with decreasing size of the elements at the rocking interfaces to model in more accuracy the impact problem according to the results of sensitivity analyses. Specifically, for a height of 0.6 m at both rocking interfaces, cubic fully integrated first-order brick elements (C3D8) of size 0.15 m are utilised. A transition zone is used for 1.0 m with C3D8 elements of size 0.3 m to pass to the coarsest mesh for the rest of the pier utilising the same type of element with size 0.45 m [19]. Fig. 2(E) presents the B31 beam element which is utilised to capture the BMs which are developed at



 



the rocking piers. The same modelling procedure with that presented in the previous sub-chapter is followed, however a different mesh scheme is generated dependent on the surrounding solid (i.e. zones with elements of 0.15 m, 0.3 m and 0.45 m). The abutment and the contribution of the abutment-backfill system are modelled as those in the conventionally isolated system, with the exception of the size of the elements for the seat of the abutments which is modified to 0.15 m, as shown in Fig. 2(F), to match the corresponding element of the deck (Fig. 2C). Fig. 2(G) shows the contact interactions which are integrated among the piers and the corresponding members (i.e. foundations and superstructure) in order to ensure rocking motion of the piers. To do so, a surface-to-surface contact with a finite sliding option is defined, assigning the "Hard Contact" and "Penalty" friction (μ = 0.9) definitions [i.a. 6, 9] given in ABAQUS [17]; the same modelling procedure for the contact between the superstructure and the abutments is followed. The boundary conditions are identical to those presented for the conventionally isolated system.

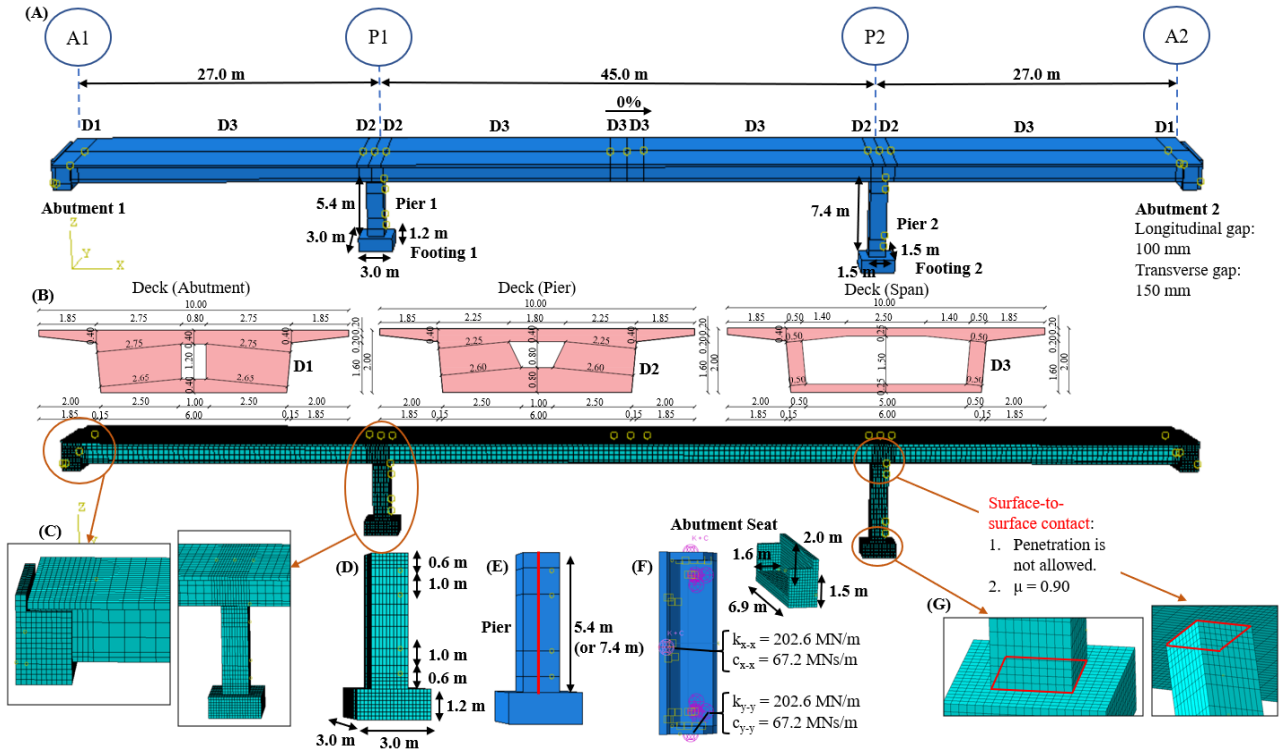


Fig. 2 – (A) Layout of the bridge with structural rocking isolation, (B) deck cross-sections, (C) superstructure mesh and mesh at the contact regions, (D) mesh of foundation-rocking pier, (E) linear beam element of the piers, (F) layout of the abutment-backfill system and (G) contact interactions to ensure rocking motion.

## 2.3 Selection and scaling of earthquake ground motions

The selection of natural records was made from the PEER NGA-West 2 database [26]. The preliminary search criteria for the selection of the records were: (i) moment magnitude ($M_w$) ranging from 6.5 to 7.0, (ii) closest distance from the recording site to the ruptured area ($R_{rup}$) between 20 km and 40 km, (iii) average shear wave velocity to a depth of 30 m ($V_{s,30}$) ranging from 350 to 600 m/s (corresponding to site conditions 'B' [16]), (iv) maximum number of ground motions from a single event limited to three and (vi) scale factor needs to be between 0.25 and 4.0. Details of the selected ground motions and the scale factors are shown in Table 1. Accordingly, Fig. 3(A) and (B) present the matching of acceleration response spectra of the scaled ground motions to the EC8 target spectrum as well as the Geometric Mean (GM) for longitudinal ($X$) and transverse ($Y$) directions, respectively. It can be seen that the GM of the scaled motions considerably overestimates the design spectrum in the plateau zone for both directions. However, with respect to the conventionally isolated system, it is observed that for the first two modes which dominate the response of the



 



structure, the response accelerations of the scaled ground motions are similar to those of the design spectrum for both directions as shown in Fig. 3.

Table 1 – Information for the ground motions selected for the dynamic response history analyses.

| Record | RSN | Scale Factor | Earthquake | Record | RSN | Scale Factor | Earthquake |
|---|---|---|---|---|---|---|---|
| R1 | 57 | 3.03 | San Fernando | R7 | 990 | 2.97 | Northridge-01 |
| R2 | 88 | 3.57 | San Fernando | R8 | 4214 | 3.36 | Niigata |
| R3 | 190 | 3.93 | Imperial Valley-06 | R9 | 5267 | 2.85 | Chuetsu-oki |
| R4 | 288 | 3.10 | Irpinia | R10 | 5776 | 3.05 | Iwate |
| R5 | 739 | 2.85 | Loma Prieta | R11 | 6971 | 2.53 | Darfield |
| R6 | 974 | 3.48 | Northridge-01 | | | | |

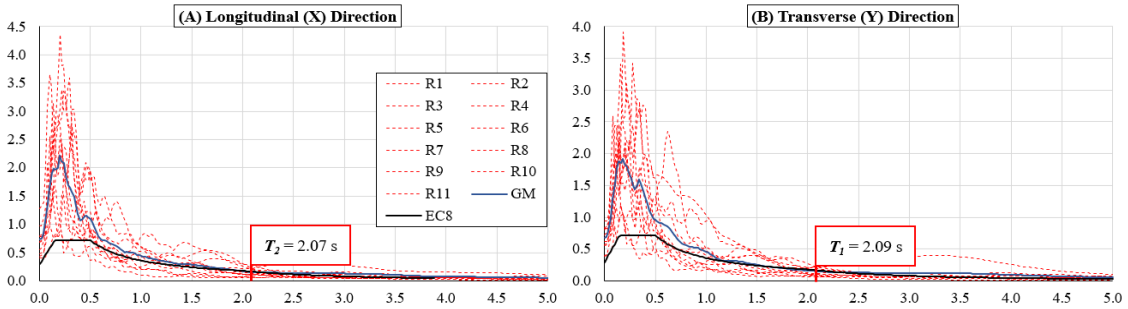


Fig. 3 – Spectral matching of the scaled response acceleration spectra to the EC8 target spectrum for (A) longitudinal (*X*) and (B) transverse (*Y*) directions.

### 2.4 Analysis process

The implicit Hilber-Hughes-Taylor (HHT) algorithm is used to integrate the system of equations of dynamic equilibrium and an automatic incrementation is selected which provides adaptation of the time-step to the requirements of the problem, while the maximum and minimum time-steps of the analyses are set equal to 0.1 s and $10^{-6}$ s, respectively.

## 3. Dynamic Response History Analyses

The bridges with conventional isolation (CI structure) and structural rocking isolation (SRI structure) are excited with the 11 pairs of scaled ground motions, separately for the longitudinal (*X*) and transverse (*Y*) directions. Fig. 4(A) summarises the peak displacements of superstructure segment (P1-P2) along the X-axis for the two isolation alternatives when subjected to the longitudinal component of the ground motions. The results for the rest of the deck sections are not presented herein for economy of space; same peak values as those presented in Fig. 4(A) were found, showing that the superstructure behaves as a rigid body longitudinally for both isolation techniques. It is observed that for 9 out of 11 records, the SRI system develops larger longitudinal deck displacements than the CI configuration with an increase that ranges from 3% to 55%. Similarly, Fig. 4(B) presents the peak transverse (*Y*) superstructure displacements for the two bridges. The results refer again to the intermediate span segment (P1-P2) which presents the highest displacements among the different deck segments for both isolation alternatives. It is observed that both systems yield comparable peak transverse displacements, and a general trend cannot be identified easily since, in some cases (6 out of 11) the SRI system reaches larger transverse displacements than the CI structure (i.e. up to 85%), while in the rest of the cases a larger displacement of the CI system occurs (i.e. up to 54%). Hence, although the two isolation techniques adopt a different design concept, the behaviour of the superstructure is fairly similar in both horizontal directions, and, therefore, the structural rocking is characterised as an isolation scheme that experiences large horizontal displacements that are comparable to those of a system with conventional seismic isolation through LRBs.



 



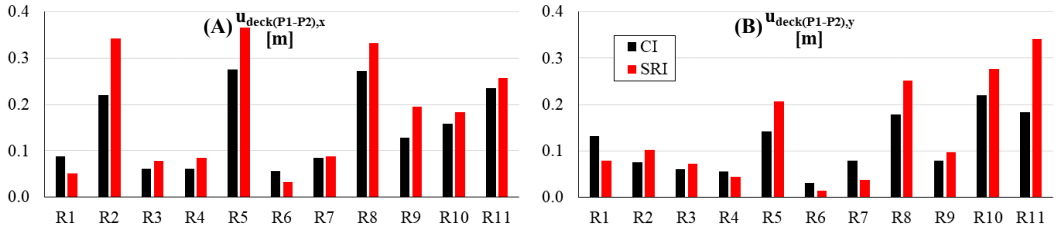


Fig. 4 – Peak (A) longitudinal (*X*) and (B) transverse (*Y*) deck displacements of segment (P1-P2) of the CI and SRI bridges subjected to the corresponding component of the ground motions (Ri).

Fig. 5(A) and (B) show the peak permanent displacements for the deck segment (P1-P2) longitudinally (*X*) and transversely (*Y*), respectively, for both isolation alternatives. It is shown that the CI structure develops permanent horizontal displacements that in 9 out of 11 cases exceed the longitudinal displacement of the SRI system, and in 10 out of 11 cases the transverse one. E.g., for the R8 record, the CI system shows a peak displacement of 100 mm and 40 mm along X-axis and Y-axis, respectively, whereas the SRI system recentres in most cases with negligible permanent displacements of approximately 10 mm. Hence, although the rocking approach is perceived as an isolation technique that experiences large horizontal displacements, similarly to a system with conventional seismic isolation, it shows negligible permanent deck displacements, even without additional recentring devices at the top rocking interfaces of the piers (e.g. bearings).

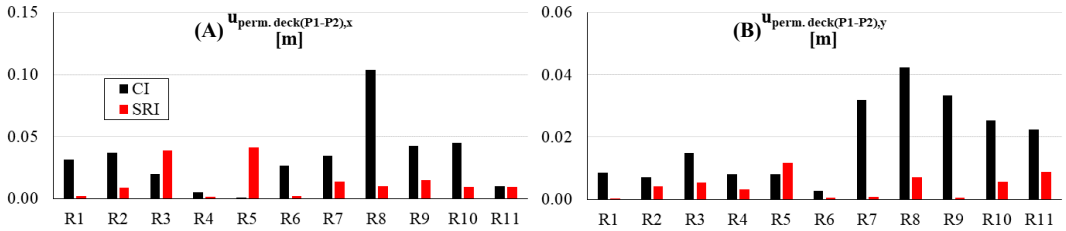


Fig. 5 – Peak permanent (A) longitudinal (*X*) and (B) transverse (*Y*) deck displacements of segment (P1-P2) of the CI and SRI bridges subjected to the corresponding component of the ground motions (Ri).

Fig. 6 shows the maximum BMs about the transverse (*Y*) direction which occur at the different spans of the superstructure for the two isolation alternatives when subjected to the longitudinal (*X*) component of all the ground motions. The BM due to the gravity loads at the different spans as well as the yield BM (same for both isolation alternatives) [20] are also presented. As expected, the BMs at the different spans of the CI structure remain unaffected by the variability of the ground motions. However, this is not the case for the SRI bridge, where the different excitations lead to differential deck uplift at the pier locations (i.e. P1 and P2), thus yielding a record-to-record variability of the response of approximately 90%. With respect to the comparison between CI and SRI bridges, it is noted that the BMs which are induced by the seismic action are considerably amplified for the SRI structure in all spans (e.g. the seismic BM for the side span (A1-P1) of the SRI system is 9 times larger than the corresponding BM of the CI system subjected to the longitudinal component of the R5 ground motion). Specifically for the end spans of the SRI system, this increase is attributed to stable seat of the deck at the abutments and the uplift of the corner piers. The same trend was observed in Agalianos *et al.* study [14] where both end spans showed similar increase of BMs. However, in this study higher increase is observed for the end span next to pier P1 (i.e. shorter) compared to the end span next to pier P2 (i.e. taller) due to the fact that the shorter piers are forced to larger uplifts than taller piers. An interesting result is found for the first time for the intermediate span (P1-P2) where increased BMs occur for the SRI bridge compared to the CI structure, which is attributed to the differential uplift of the superstructure at the pier locations. It is observed that for the longitudinal component of the R5 ground motion, the maximum BM at the intermediate span (P1-P2) almost approaches the yield BM of the section; therefore, special attention must be paid to the integrity of the deck in asymmetric rocking systems.



 



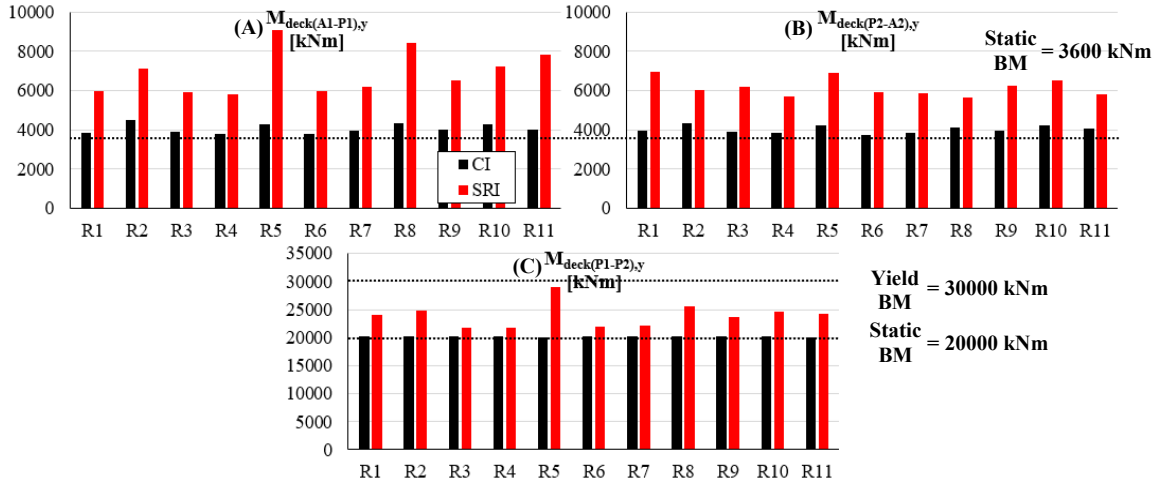


Fig. 6 – Maximum BMs about the transverse (*Y*) direction at (A) the side span (A1-P1) and (B) the side span (P2-A2) as well as (C) the intermediate span (P1-P2) of the CI and SRI bridges subjected to the longitudinal (*X*) component of the ground motions (Ri).

Fig. 7 shows the peak drifts of pier P2 which occur longitudinally (*X*) and transversely (*Y*) for the two isolation perspectives; the results for pier P1 show similar trends as those in Fig. 7. As expected, the rocking pier P2 of the SRI system reaches very large drifts (i.e. up to 5%) compared to the corresponding pier of the CI structure (merely reaches 0.3%), which is in agreement with several experimental works [i.a. 12]. Despite the large drift, the rocking pier does not fail by exceeding the overturning threshold which approximately corresponds to 20% drift (i.e. the resultant of the pier does not fall outside the footprint of the pier). The piers' movement in the SRI system is mainly accommodated by rigid body motion and the flexural response is minimal, as shown in previous works [e.g. 14]. Nevertheless, the bending component of the rocking piers needs to be addressed. Fig. 8(A) presents the linear beam element of the piers as well as three different sections (i.e. 1-Bottom, 2-Middle and 3-Top) which are considered to examine locally the bending behaviour of each pier. The peak pier P1 BMs with respect to the Y-axis are presented for the three different sections as shown in Fig. 8(B), (C) and (D) for both CI and SRI structures when subjected to the longitudinal (*X*) component of the ground motions. Interestingly, the rocking pier P1 of the SRI system shows BMs which are locally higher than those of the corresponding member of the CI system, hence indicating that flexure is more critical in the rocking pier than in the conventional isolation. Specifically, the BMs at section 1 (Bottom) are higher for the rocking pier than the CI one in 7 out of 11 cases, reaching values which are approximately 2.5 times larger. This behaviour becomes more significant at section 3 (Top) of the pier where the BMs for P1 of the SRI system are almost 18 times larger than those of the CI system. On the contrary, in section 2 (middle), the conventional pier shows higher BMs in 10 out of 11 cases. Thus, the rocking elements indicate the presence of regions (i.e. bottom and top, or close to the rocking interfaces) where bending is significantly high and has to be accounted for in reinforcement design. The results for BMs about the longitudinal (*X*) direction for P1 and both components for P2 are not discussed herein, however, the trends are identical to those presented for P1.

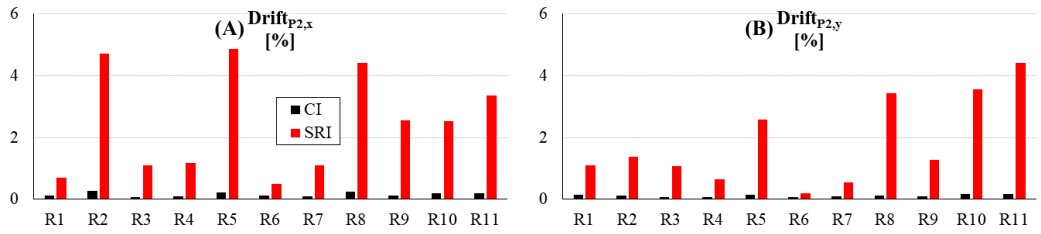


Fig. 7 – Peak pier P2 (A) longitudinal (*X*) and (B) transverse (*Y*) drifts of the CI and SRI bridges subjected to the corresponding component of the ground motions (Ri).



 



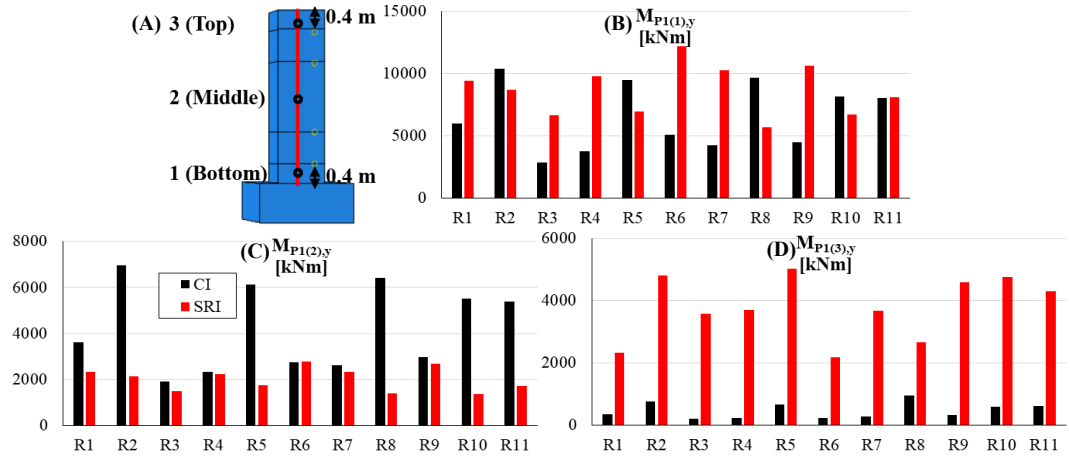


Fig. 8 – (A) Linear beam element of the piers and location of the examined pier sections (*1-Bottom, 2-Middle, 3-Top*) as well as peak pier P1 BMs about the transverse (*Y*) direction at sections (B) 1, (C) 2 and (D) 3 of the CI and SRI bridges subjected to the longitudinal (*X*) component of the ground motions (Ri).

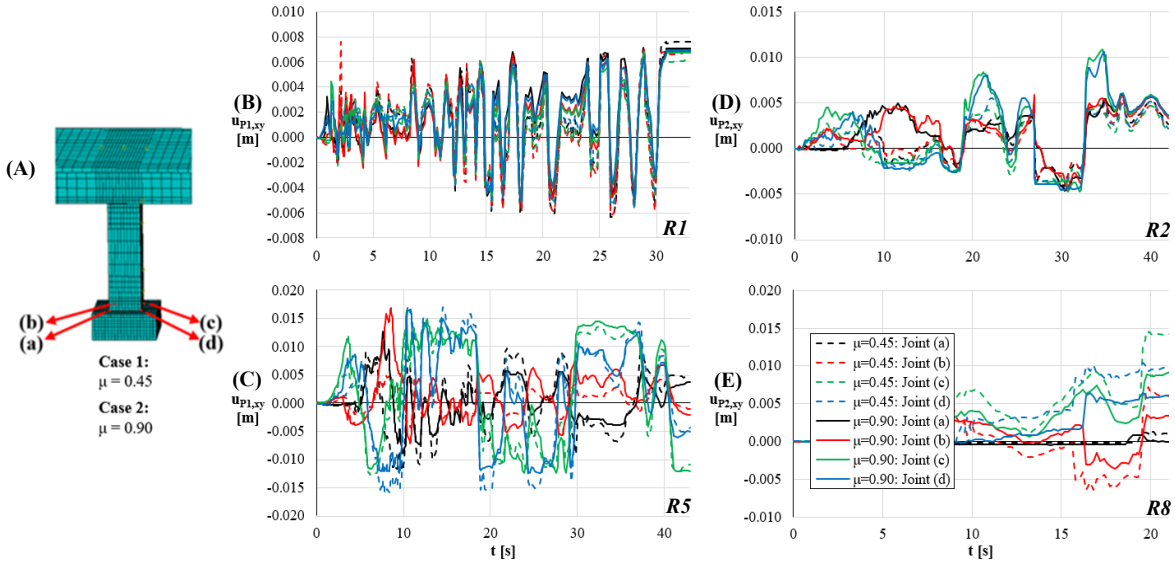


Fig. 9 – (A) Configuration of the corner joints at the bottom of the pier (*a, b, c, d*) of the SRI bridge and histories of total horizontal displacements of pier P1 subjected to the (B) R1 and (C) R5 ground motions and of pier P2 subjected to the (D) R2 and (E) R8 ground motions for different values of coefficient of friction $\mu$.

A crucial issue for the free-standing rocking piers studied herein is their adequacy to provide sufficient recentring capacity after a strong seismic event, given that sliding can occur in this type of analysis and no measurements were undertaken intentionally to minimise permanent displacements (e.g. additional devices [i.a. 6, 15] and/or grooves [i.a. 1, 2]). Apart from the FE model with $\mu$ = 0.9 for the rocking interfaces, an additional model with $\mu$ = 0.45 (i.e. with a safety factor of 2) is considered to examine the effect of coefficient of friction value in recentring capability of rocking piers. The four corner joints at the bottom of each rocking pier, as shown in Fig. 9(A), are utilised to trace potential residual displacements, as well as twisting of the element with respect to its initial position. In this analysis, the two components of each ground motion are applied simultaneously to the footings in order to derive the total horizontal displacement of each node. Fig. 9(B) and (C) present the histories of total horizontal displacements of the four bottom joints of P1 when subjected to R1 and R5 ground motions, respectively, for both values of coefficient of friction $\mu$. In the first case, it can be seen that the two different values of $\mu$ affect negligibly the rocking response of P2, yielding equivalent histories throughout the whole motion, however for $\mu$ = 0.9 the pier is



 



only shifted approximately 7 mm with zero twisting, while for the conservative value (i.e. $\mu$ = 0.45) the pier also twists approximately 0.04° with respect to its initial position. In the second case, the permanent horizontal displacements are similar for the piers with different tangential behaviour in the interface conditions, resulting in shifting and twisting of approximately 12 mm and 0.23°, respectively. Similarly, Fig. 9(D) and (E) present a shift and twist condition of the taller pier (P2) for the different values of $\mu$. Specifically, the taller pier is shifted approximately 3 mm for the R2 ground motion for both values of coefficient of friction. On the other hand, conservativeness in the value of $\mu$ shows larger permanent displacements of P2 for the R8 ground motion by shifting 14 mm and twisting about 0.19° compared to $\mu$ = 0.9 where the corresponding values are 9 mm and 0.1°. Thus, both piers are displaced negligibly with respect to their initial positions, indicating that a free-standing rocking configuration is capable of providing sufficient recentring capacity. Additionally, although slightly larger permanent displacements are detected in some cases when a conservative value of $\mu$ is considered in analysis, the overall performance does not seem to be affected considerably.

## 4. Conclusions

The present study used a variant of an existing asymmetric overpass to compare the seismic performance of two different isolation techniques, i.e. conventional isolation through LRBs and structural rocking isolation. The conventionally isolated configuration is redesigned according to the current EC8 provisions and the rocking isolation alternative adopts realistic interface conditions and a purely free-standing scheme for the rocking piers (i.e. without utilising any additional devices/members). To this purpose, 3D numerical models of the entire bridge system were developed in ABAQUS, and linear dynamic analyses were performed. Eleven pairs of scaled earthquake records to match the design spectrum of EC8 were used to examine the potential advantages and obstacles of the rocking alternative. The results show large horizontal deck displacements for both systems despite the different isolation 'philosophy'. However, the superstructure of the rocking system recentres almost completely in most of the examined cases and shows smaller residual displacements than those of the conventionally isolated system, which nonetheless are within the EC8-2 prescribed limits. The superstructure of the rocking system shows considerably higher BMs at the end spans than those of the conventionally isolated system. This is attributed to the significant uplift of the deck at the position of the rocking piers and to the zero uplift at the position of the abutments. Hence, the larger the uplift of the pier, the higher the increase in the BM at the end spans and, therefore, the higher the BM demand at the end span next to the shortest rocking pier. An interesting observation is made for the first time, i.e. that the differential uplift of the unequal height piers is also responsible for the increased BMs at the intermediate span, compared to the conventionally isolated case. Hence, the behaviour of the superstructure is critical in rocking structures, especially in asymmetric configurations where rocking behaviour leads to several disadvantages in a design context. The rocking piers show a rigid body motion with considerably higher drifts than those of the conventionally isolated system, although the structure remains stable. However, increased BMs occur locally in the piers of the rocking bridge, and close to the rocking interfaces. Therefore, the reinforcement design of the rocking piers may need to follow the procedure followed for conventional piers at least in the regions wherein bending is critical. On the other hand, after the earthquake the rocking piers return to their at-rest position without the need for additional devices, while negligible permanent displacements and rotations were observed independently on the value of the coefficient of friction. Nevertheless, it is noted that the vertical component of the ground motions which can be detrimental in terms of recentring capability is ignored herein. Hence, although structural rocking seems to be an isolation technique that is safer than conventional isolation in bridges from the collapse prevention point of view, several issues have to be addressed in the design of structural members, and special attention needs to be paid to their detailing.

## 5. References

[1] Thomaidis IM, Kappos AJ, Camara C (2019a): Dynamics and seismic stability of planar symmetric rocking bridges. *2nd International Conference on Natural Hazards and Infrastructure*, Chania, Greece.



 




[2] Thomaidis IM, Kappos AJ, Camara C (2019b): Dynamics of planar asymmetric rocking bridges including the abutment contribution. *SECED: Earthquake Risk and Engineering towards a Resilient World*, Greenwich, London.

[3] Vassiliou MF (2017): Seismic response of a wobbling 3D frame. *Earthquake Engineering and Structural Dynamics*, 1-17.

[4] Mohamad ME, Ibrahim IS, Abdullah R, Rahman AB, Kueh ABH, Usman J (2015): Friction and cohesion coefficients of composite concrete-to-concrete bond. *Cement & Concrete Composites*, **56**, 1-14.

[5] Roh HS, Reinhorn AM (2009): Analytical modelling of rocking elements. *Engineering Structures*, **31**, 1179-1189.

[6] Sideris P (2015): Nonlinear quasi-static analysis of hybrid sliding-rocking bridge columns subjected to lateral loading. *Engineering Structures*, **101**, 125-137.

[7] Palermo A, Pampanin S, Calvi GM (2004): Use of "controlled rocking" in the seismic design of bridges. *13th World Conference on Earthquake Engineering*, Vancouver, Canada.

[8] Chen Y, Liao W, Lee C, Wang Y (2006): Seismic isolation of viaduct piers by means of a rocking mechanism. *Earthquake Engineering and Structural Dynamics*, **35**, 713-736.

[9] ElGawady MA, Dawood HM (2012): Analysis of segmental piers consisted of concrete filled FRP tubes. *Engineering Structures*, **38**, 142-152.

[10] Palermo A, Pampanin S, Calvi GM (2005): Concept and development of hybrid solutions for seismic resistant bridge systems. *Journal of Earthquake Engineering*, **9** (6), 899-921.

[11] Makris N, Vassiliou MF (2014): Are some top-heavy structures more stable?. *Journal of Structural Engineering*, **140** (5).

[12] ElGawady MA, Sha'Ian A (2011): Seismic behavior of self-centering precast segmental bridge bents. *Journal of Bridge Engineering*, **16** (3), 328-339.

[13] Aviram A, Mackie KR, Stojadinovic B (2008): Effect of abutment modelling on the seismic response of bridge structures. *Earthquake Engineering and Engineering Vibration*, **7**, 395-402.

[14] Agalianos A, Psychari A, Vassiliou MF, Stojadinovic B, Anastasopoulos I (2017): Comparative assessment of two rocking isolation techniques for a motorway overpass bridge. *Frontiers in Built Environment*, **3** (47).

[15] Dimitrakopoulos EG, Giouvanidis AI (2015): Seismic response analysis of the planar rocking frame. *Journal of Engineering Mechanics*, **141** (7).

[16] CEN (2004): Eurocode 8: Design of Structures for Earthquake Resistance (EN1998). *CEN*, Brussels, Belgium.

[17] ABAQUS 6.14 (2012): Standard user's manual. Providence. *RI: Dassault Systèmes Simulia Corporation*, ETH Zürich, Switzerland.

[18] EAK2003 (2003): Greek seismic code. Athens, Greece.

[19] Baker M (2018): How to get meaningful and correct results from your finite element model. *Technical University of Braunschweig*, Braunschweig, Germany.

[20] Gkatzogias KI (2017): Performance-based seismic design of concrete bridges for deformation control through advanced analysis tools and control devices. *Doctor of Philosophy Thesis, City, University of London*, London, UK.

[21] Caltrans (2013): Seismic design criteria version 1.7. *California Department of Transportation*, Sacramento, USA.

[22] Mylonakis G, Nikolaou S, Gazetas G (2006): Footings under seismic loading: Analysis and design issues with emphasis on bridge foundations. *Soil Dynamics and Earthquake Engineering*, **26**, 824-853.

[23] Naeim F, Kelly JM (1999): Design of seismic isolated structures: From theory to practice. *Wiley*, New York, USA.

[24] Constantinou MC, Kalpakidis I, Filiatrault A, Ecker Lay RA (2011): LRFD-based analysis and design procedures for bridge bearings and seismic isolators. *Technical Report MCEER*, New York, USA.

[25] Van Engelen NC, Kelly JM (2015): Correcting for the influence of bulk compressibility on the design properties of elastomeric bearings. *Journal of Engineering Mechanics*, **141** (6), 1–11.

[26] Ancheta DT, Darragh RB, Stewart JP, Seyhan E, Silva WJ, Chiou BSJ, Wooddell KE, Graves RW, Kottke AR, Boore DM, Kishida T, Donahue JL (2013): PEER NGA-West 2 Database., USA. http://ngawest2.berkeley.edu/.



 